

Article

Reaction Layer Analysis of In Situ Reinforced Titanium Composites: Influence of the Starting Material Composition on the Mechanical Properties

Isabel Montealegre-Meléndez ¹, Cristina Arévalo ^{1,*}, Ana M. Beltrán ¹,
Michael Kitzmantel ², Erich Neubauer ² and Eva María Pérez Soriano ¹

¹ Escuela Politécnica Superior, Universidad de Sevilla, Calle Virgen de África, 7, 41011 Sevilla, Spain; imontealegre@us.es (I.M.-M.); abeltran3@us.es (A.M.B.); evamps@us.es (E.M.P.S.)

² RHP Technology GmbH, 2444 Seibersdorf, Austria; m.ki@rhp.at (M.K.); e.ne@rhp.at (E.N.)

* Correspondence: carevalo@us.es; Tel.: +34-954-482-278

Received: 30 January 2020; Accepted: 15 February 2020; Published: 18 February 2020



Abstract: This study aims at the analysis of the reaction layer between titanium matrices and reinforcements: B₄C particles and/or intermetallic Ti_xAl_y. Likewise, the importance of these reactions was observed; this was particularly noteworthy as regard coherence with the obtained results and the parameters tested. Accordingly, five starting material compositions were studied under identical processing parameters via inductive hot pressing at 1100 °C for 5 min in vacuum conditions. The results revealed how the intermetallics limited the formation of secondary phases (TiC and TiB) created from the B and C source. In this respect, the percentages of TiB and TiC slightly varied when the intermetallic was included in the matrix as prealloyed particles. On the contrary, if the intermetallics appeared in situ by the addition of Ti-Al powder in the starting blend, their content was lesser. The mechanical properties values and the tribology behaviour might deviate, depending on the percentage of the secondary phases formed and its distribution in the matrix.

Keywords: in situ composites; inductive hot pressing; tribology; titanium composites; reaction layer; intermetallics

1. Introduction

The interest of materials with high specific properties and good tribological behaviour raises the needs in terms of improving the properties of materials like titanium and its alloys. In the fields of aerospace, military industry and biomedicine, the use of these materials is very popular [1–4]; however, nowadays, there are limitations regarding their mechanical and poor tribological properties. Therefore, titanium matrix composites (TMCs) are valued as materials that combine low density with mechanical properties [5–8]. Presently, there is a great variety of reinforcements employed in these composites. The most popular ones showed in diverse research works tend to increase the hardness, Young's modulus and the tribological behaviour without incrementing the density. As examples, it may include TiB₂, TiB, TiC, B, B₄C, carbon nanotubes, graphite and nanodiamonds [9–12]. Among these materials, B₄C ceramic particles have been presented in investigations as an optimal form to obtain B and C sources to origin in situ TiB and TiC [13–16]. In this regard, these secondary phases play a key role in the strengthening of the titanium matrices [17]. The main advantage of these in situ phases resides in the existence of a good interfacial bonding of the reinforcement-matrix. Moreover, the ceramic reinforcements formed during in-situ processing are finer, more thermodynamically stable and uniform in size distribution in the metal matrix [18,19]. Therefore, the study of the reaction layer between the matrix and the particles is important in order to achieve a better understanding of

the cause that could promote or not these reactions and their products. While there is considerable literature on the grounds of strengthening and the reaction mechanisms [20,21], there are only a few studies where the reaction layer is analysed. It is also investigated how the presence of Ti_xAl_y as intermetallic in the titanium matrices could affect the final appearance of these secondary phases (TiB and TiC) [22–24]; however, the reaction layer in the presence of intermetallic, as well as its decomposition, has been little studied [25,26]. Hence, here lies the importance for understanding and determining the evolution of the reaction layer with B_4C particles and intermetallics Ti_xAl_y and how these layers and the final properties of the consolidated composites could be affected by the combination of the starting materials. Therefore, this research aims not only to study the reaction layer but also to investigate and characterise TMCs from five different blends. These blends were designed and processed considering interesting combinations of starting powders, in order to observe the regarding properties and the above-mentioned reaction layer phenomenon. Through the selection of the diverse intermetallic starting powders, variations in the behaviour of the TMCs may be expected.

In several investigations concerning the manufacture of titanium composites via powder metallurgy (PM) [27,28], inductive hot pressing (iHP) is considered as a suitable fabrication option due to its flexibility and short cycles. For that reason, and thanks to the experience of the authors on TMCs manufacturing, the fabrication route of the specimens was through iHP. In preliminary studies [29,30], an inflexion temperature, at which secondary phases were formed in situ, was observed. The analysis of the reaction layer has been carried out in specimens produced at this inflexion temperature (1100 °C) in vacuum conditions.

Hence, the five specimens were in detail characterised through scanning and scanning-transmission electron microscopies (SEM and (S)TEM) and by X-ray diffraction analysis (XRD). Furthermore, their tribological and physical properties were measured and evaluated. In this regard, the relation between the starting materials and the final properties was thoroughly investigated.

2. Materials and Methods

2.1. Materials

The starting blends were five different combinations of powders, using only one titanium matrix powder, as listed in Table 1.

Table 1. Summary of the composition of the tested specimens.

Blend	Materials	B_4C [Volume %]	Ti:Al [Volume %]
1	Ti + B_4C	30	-
2	Ti + B_4C + Ti-Al(1)	30	20
3	Ti + Ti-Al(1)	-	20
4	Ti + B_4C + Ti-Al(2)	30	20
5	Ti + Ti-Al(2)	-	20

The powders employed in this research were previously characterised through particle size distribution and morphological analysis, in order to verify their supplied information. The Mastersizer 2000 (Malvern Instruments, Malvern, UK) equipment was used to determinate the average particle size, and their morphology study was performed by SEM from FEI Teneo images (FEI, Eindhoven, Netherlands).

Titanium powder was produced by TLS GmbH (Bitterfeld, Germany); it showed a spherical morphology in agreement with the manufacturer's information, being its mean diameter of 109 μm . The B_4C particles were manufactured by ABCR GmbH & Co KG (Karlsruhe, Germany) with an average size diameter of 64 μm ; the morphology of these ceramic particles was irregular and with slightly sharp edges.

Concerning the intermetallic powders, there were substantial differences between the two selected. The one named Ti-Al(1) was a prealloyed Ti_3Al and $TiAl_3$ intermetallic powder manufactured by TLS GmbH (Bitterfeld, Germany). This Ti-Al(1) showed a spherical morphology, and its mean diameter was around $75\ \mu m$. The other intermetallic powder used was named Ti-Al(2). It was made from a blend of elementary Al (NMD GmbH, Heemsen, Germany; $9\ \mu m$) and Ti fine powder with a mean diameter of $29\ \mu m$ in molar ratio 1:1 by TLS GmbH (Bitterfeld, Germany) [22,30].

In addition to the starting materials' characterisations, XRD analysis was accomplished—Bruker D8 Advance A25 (Billerica, MA, USA) with $Cu-K\alpha$ radiation. Figure 1 shows the patterns of the powders from which the five blends were prepared. Based on the resulted diffraction spectra, the composition of the powders agreed with the suppliers' information in the case of Ti powder, B_4C and Ti-Al(1) in Figure 1a–c, respectively. In the case of Ti-Al(2), the remarked peaks corresponded to the Ti and Al elements, matching the elementary blending of Ti and Al, whose molar ratio was 1:1 (Ti:Al), as it was above-mentioned.

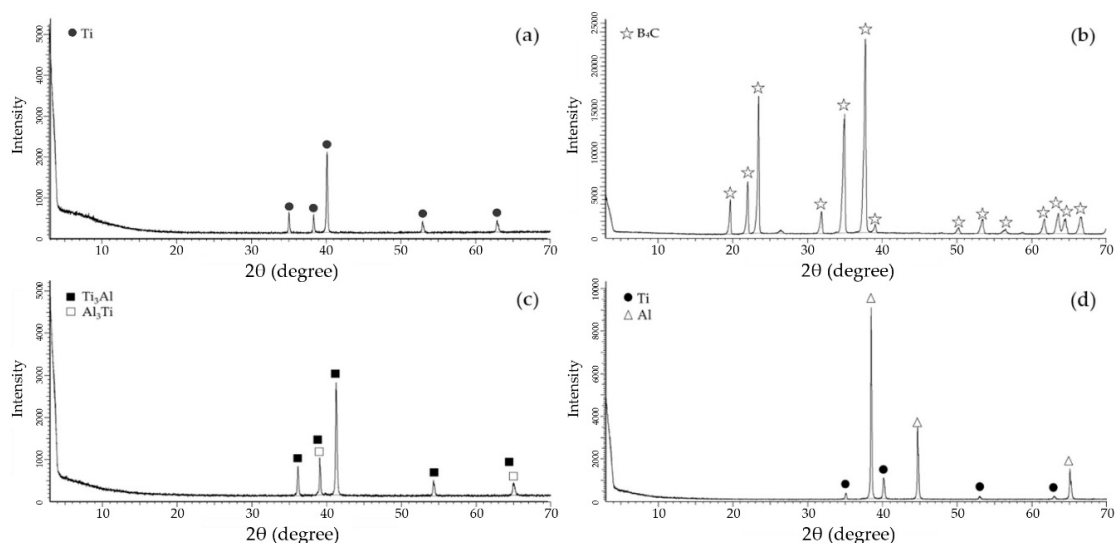


Figure 1. XRD (X-ray diffraction) patterns of the starting powders: (a) Ti powder, (b) B_4C particles, (c) Ti-Al(1) powder and (d) Ti-Al(2) powder.

2.2. Methods

After the blending preparation, similar as in previous authors' works [30], the consolidation of the specimens via iHP was performed, employing a self-made inductive hot-pressing machine; equipment from RHP-Technology GmbH (Seibersdorf, Austria).

This machine provided the time of the operational cycles to be reduced thanks to its advantageous high heating rate. The time set was 5 min in vacuum conditions at $1100\ ^\circ C$ and 80 MPa. The same procedure to fill the die was carried out for the consolidation of each specimen [30]. The graphite die for all the iHP cycles had a diameter of 20 mm. A detailed description of the manufacturing process was reported in previous authors' work [22].

The consolidated composites were studied at length. After thorough metallographic preparation, their microstructures were examined by SEM at 15 kV. The (S)TEM characterisation was carried out using a FEI Talos F200S microscope (FEI, Eindhoven, Netherlands) operating at an accelerating voltage of 200 kV and equipped with a super-X energy-dispersive X-ray spectrometry (EDX) system, which includes two silicon drift detectors. The elemental mapping experiments were accomplished by combining high-angle annular dark-field imaging (HAADF) and EDX acquisition in (S)TEM mode. The mechanical grinding and ion milling procedures were performed for the (S)TEM studies following standard procedure for TEM lamella preparation. Moreover, an XRD analysis was conducted to identify the diverse crystalline phases in the TMCs. Ultrasonic method (Olympus 38 DL, Tokyo, Japan) was

used to calculate Young's modulus by measuring longitudinal and transverse propagation velocities of acoustic waves [31]. The densification of the specimens was measured according to the Archimedes' method [32]. The relative density was computed as the ratio of the compacts' density to their theoretical values of the given material, determined by the rule of mixtures. A test model, Struers-Duramin A300 (Ballerup, Germany), was used to ascertain the Vickers hardness (HV2). The hardness measurements took place on the polished cross-section of the specimens. The reported values were the average of eight indentations.

After the characterisation of the specimens, the tribological behaviour was studied. Before running the tests, the specimens were prepared (grinded and polished), cleaned with acetone in an ultrasonic bath and, after that, dried. The wear behaviour of the TMCs was conducted in a ball-on-disc tribometer (Microtest MT/30/NI, Madrid, Spain) using alumina balls with a diameter of 6 mm. At room temperature, the normal load of 3 N on the ball with a sliding speed of 125 mm/s was employed to measure the wear properties. It was tested at a sliding distance of 500 m on the specimens' surface, with a circular path of 3 mm in radius. The results were analysed at similar conditions in order to compare and evaluate the influence of the starting materials. The morphology of the worn surfaces was characterised by optical microscopy with a Leica Zeiss DMV6 (Leica Microsystems, Heerbrugg, Switzerland).

3. Results and Discussion

3.1. Microstructural Study and XRD Analysis

The microstructural study revealed significant differences related to the starting powders employed. Figure 2 displayed a microstructure general overview of the specimens. The circular backscattered (CBS) SEM images in Figure 2a,b,d showed how the B_4C particles were homogeneously distributed in the titanium matrices.

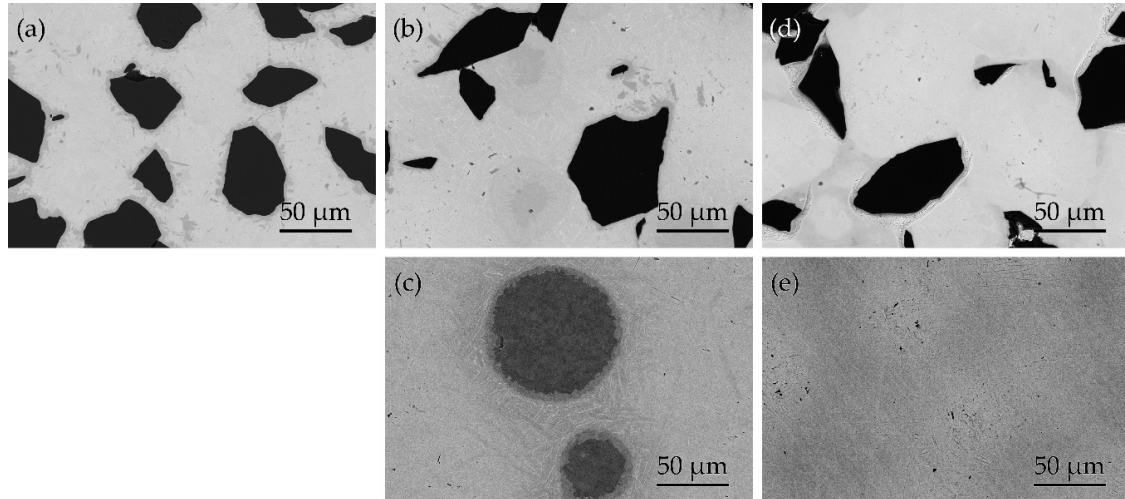


Figure 2. CBS-SEM (circular backscattered-scanning electron microscopy) images: (a) Ti + 30 vol. % B_4C , (b) Ti + 30 vol. % B_4C + 20 vol. % Ti-Al(1), (c) Ti + 20 vol. % Ti-Al(1), (d) Ti + 30 vol. % B_4C + 20 vol. % Ti-Al(2) and (e) Ti + 20 vol. % Ti-Al(2).

The different shades of grey close to these ceramic particles suggested the presence of in situ secondary phases. However, at this scale, that was not easily appreciated. Conversely, in the case of the specimen made from Ti only with Ti-Al(1) (Figure 2c), the dark grey areas corresponded to the intermetallic phases (Figure 2c). The intermetallics in the matrix were visible and recognised as spherical precipitates with degradation around. However, if there were Ti-Al powders employed in the starting mixing as Ti-Al(2), the location of the phases rich in Al was not appreciated (Figure 2e). Although, in the bibliography has been reported the formation of new phases due to the liquid metal dealloying reaction [33,34], in this specimen fabricated at this temperature, it seems that no

intermetallics were in situ formed, having the aluminium in solid solution with the titanium matrix. These observations were verified by the XRD analysis.

The microstructural characterisation at higher magnification is presented in Figure 3, revealing several phases depending on the starting materials. Evaluating the area surrounding the B_4C particles, there were significant variations in the volume and thickness of the in situ secondary phases formed in the reaction layer. In the TMC without intermetallic addition, more in situ secondary phases were formed (Figure 3a). The incorporation of Ti_xAl_y in the starting powders of the TMCs not only modified the microstructure of the specimens but also affected the secondary phases formed, whereupon the final properties of the specimens could suffer variations. A detailed study of the TMCs' microstructure evolution contributed to a better understanding of in situ formed phases, as well as the distribution of the Ti_xAl_y in the titanium matrices. In Figure 3a,b,d, the reaction layer around the B_4C could be observed, being mainly composed of B and TiB. These TiB phases could also appear further from the B_4C particles when no intermetallic was used, as well as TiC (Figure 3a,b). It suggested that the employ of Ti-Al intermetallic in the initial blending involved a slight obstacle in the origin of in situ formed phases. The Al could act as a barrier, blocking the reactions between the Ti and the B and C sourced by the B_4C particles. This phenomenon was more visible in the sample with Al as an elementary powder (TiAl(2), Figure 3d). The morphology of in situ phases will be discussed later.

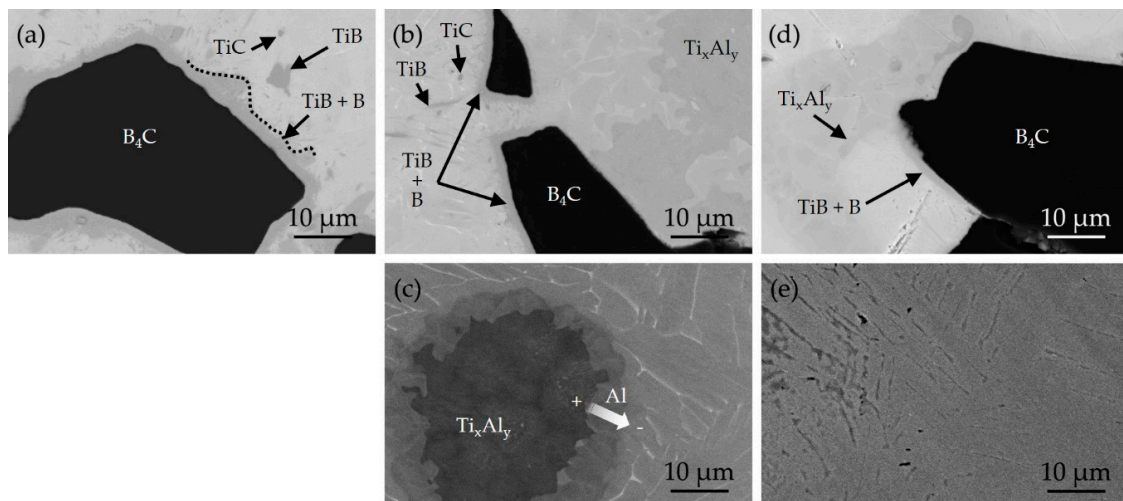


Figure 3. Phases identification via CBS-SEM images: (a) Ti + 30 vol. % B_4C , (b) Ti + 30 vol. % B_4C + 20 vol. % Ti-Al(1), (c) Ti + 20 vol. % Ti-Al(1), (d) Ti + 30 vol. % B_4C + 20 vol. % Ti-Al(2) and (e) Ti + 20 vol. % Ti-Al(2).

As previously mentioned, when no B_4C was added, how introducing Ti_xAl_y in the matrix caused differences. This can be clearly seen in Figure 3c,e. There was a reaction layer surrounding the intermetallic phases when prealloyed intermetallic was introduced as a starting powder (TiAl(1)). This reaction layer was due to the decomposition of the intermetallic being Al-incorporated into the matrix.

In order to understand TMCs with B_4C particles in detail, the reaction layer and secondary phases were analysed by TEM and (S)TEM (Figures 4–6). In the reaction layer, the in situ formed precipitates could be recognised. The more the presence of Al in the matrix, the thicker the reaction layer was observed. The reason, as previously discussed, could be the diffculted diffusion of B and C elements into the matrix. Next to the B_4C particles, the size of TiB and TiC in situ secondary phases created were smaller to grow as moving away from the ceramic particles. When Al was not present in the matrix, secondary phases were bigger in size (Figure 4a).

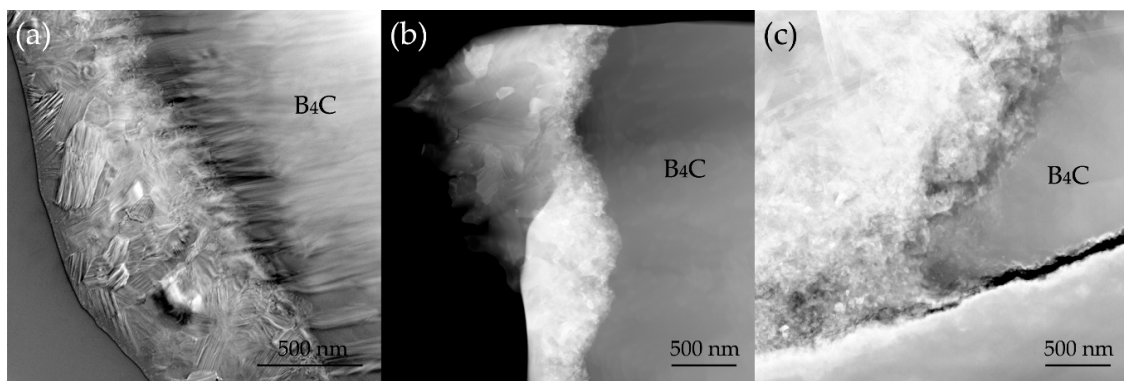


Figure 4. TEM (transmission electron microscopies) images: (a) Ti + 30 vol. % B_4C , (b) Ti + 30 vol. % B_4C + 20 vol. % Ti-Al(1) and (c) Ti + 30 vol. % B_4C + 20 vol. % Ti-Al(2).

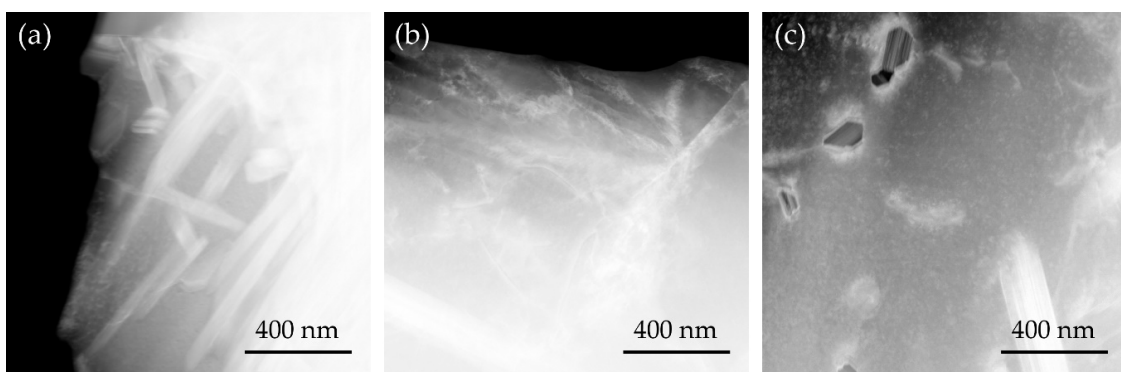


Figure 5. (S)TEM images 80,000x: (a) Ti + 30 vol. % B_4C , (b) Ti + 30 vol. % B_4C + 20 vol. % Ti-Al(1) and (c) Ti + 30 vol. % B_4C + 20 vol. % Ti-Al(2).

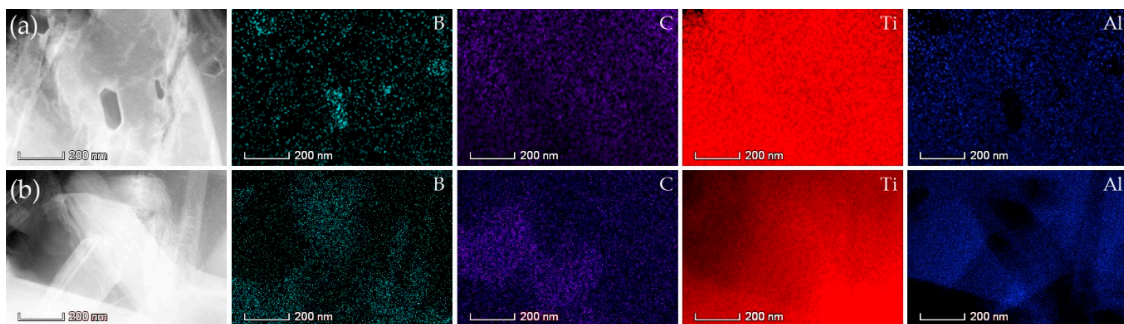


Figure 6. TEM images and compositional mappings: (a) Ti + 30 vol. % B_4C + 20 vol. % Ti-Al(1) and (b) Ti + 30 vol. % B_4C + 20 vol. % Ti-Al(2).

In Figures 4 and 5, the observed phases consisted in TiB and TiC were recognised due to their well-known morphology, as whiskers in the case of TiB and as isolated grey areas for TiC from its dendritic formation [30]. In TMCs reinforced only by B_4C , the morphologies of TiB and TiC phases could be more easily identified (Figure 4a), while for TMCs with B_4C and intermetallic, these precipitates were not clearly observed (Figure 4b,c). Figure 5 shows the formation of precipitates far from the B_4C particles. The lower the content of Al as a solid solution in the matrix, the higher the concentration of secondary phases in these areas was found. In this way, this was more significant with Ti-Al(2) (Figure 5c) than with Ti-Al(1) (Figure 5b), confirming SEM microscopy.

Concluding the microstructural characterisation, a compositional mapping of the main present elements in samples with B_4C and intermetallic was performed (Figure 6). The aim was to study the composition of the smallest precipitates to check if there were other formed secondary phases,

apart from the expected TiB and TiC. The results confirmed that there was no reaction between the B and C particles with Al.

The XRD patterns of the specimens are illustrated in Figure 7. The one of TMCs without intermetallic (Figure 7a) was intended to serve as a reference on the comparison in terms of precipitates formation regarding the specimens with Ti-Al(1) (Figure 7b) and Ti-Al(2) (Figure 7d). The peaks of B₄C could clearly be identified in these three patterns. The variations in the peaks of the in situ formed TiB and TiC that were related to the intermetallic powder employed as the starting powder were meaningful in the results. It suggested that the reaction of the matrix and the ceramic particles was more decelerated if the starting powder was made from an elementary blending of Ti-Al. The peaks corresponding to the TiAl₃ phase were not visible in the XRD patterns. These results were in agreement with the microstructures observed by SEM and (S)TEM.

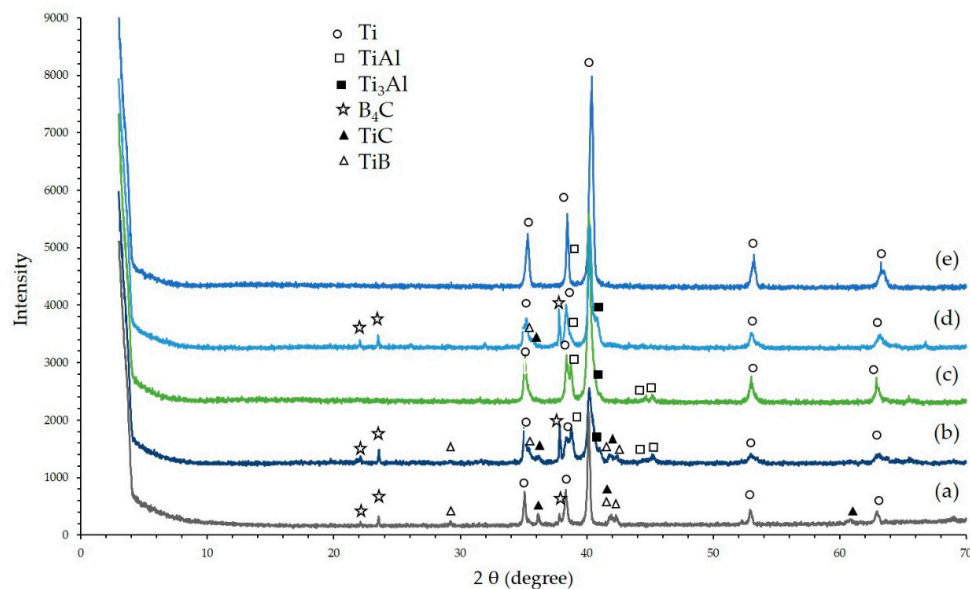


Figure 7. XRD patterns of the specimens: (a) Ti + 30 vol. % B₄C, (b) Ti + 30 vol. % B₄C + 20 vol. % Ti-Al(1), (c) Ti + 20 vol. % Ti-Al(1), (d) Ti + 30 vol. % B₄C + 20 vol. % Ti-Al(2) and (e) Ti + 20 vol. % Ti-Al(2).

When the starting blend was made without B₄C, while the pattern of the specimen produced from intermetallic powder Ti-Al(1) revealed the peaks of the Ti₃Al and TiAl phases (Figure 7c), the pattern of the specimens made from Ti-Al(2) powder showed mainly the displaced peaks of Ti and a small quantity of TiAl (Figure 7e). This could be due to the Al migrated into the titanium crystal lattice, avoiding the formation of Ti_xAl_y phases. The presence of B₄C and the secondary phases affected the Al diffusion; therefore, the peak of Ti₃Al was slightly detected in specimens made from B₄C and Ti-Al(2) (see Figure 7d).

3.2. Physical and Tribological Properties

The values of hardness in the matrix and Young's modulus are plotted in Figure 8. These results agreed with the previously commented microstructural study and XRD analysis. As it was expected, the B₄C addition led to the onset of TiB and TiC becoming in an increase of the hardness and Young's modulus. Whereas there was more evidence of the TiB and TiC precipitates in the composites made from Ti-Al(1), the hardness and Young's modulus of these specimens were similar to the composites made from elementary Ti-Al powder (Ti-Al(2)). The Al diffusion phenomenon into the titanium crystal lattice was helping to the matrix strengthening in specimens made from Ti-Al(2). Comparing samples without B₄C, the same trend was observed in the hardness and Young's modulus values (Figure 8). Therefore, this verified how, from different starting powders and diverse reactions

phenomenon, the final properties could be, to some extent, similar; other authors have reported some positive or negative effects on the mechanical behaviour of the titanium alloys with other intermetallic additions [35,36].

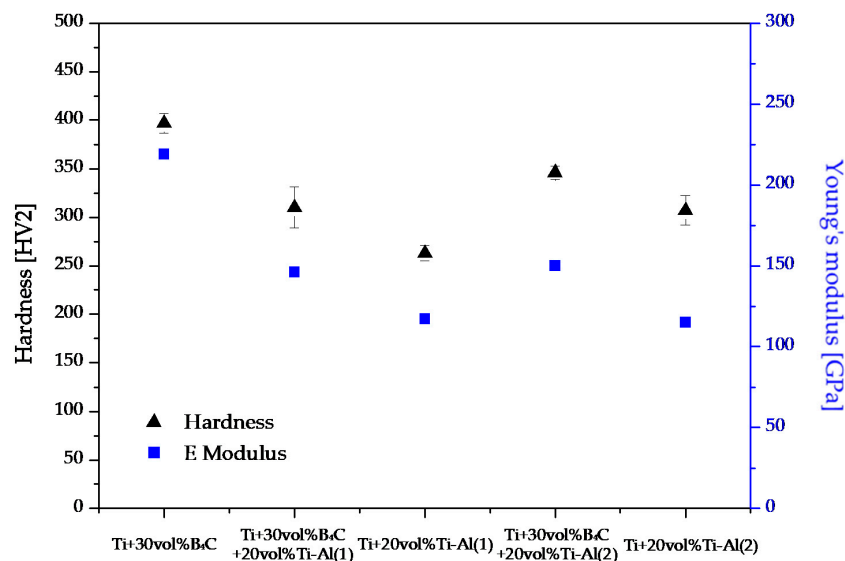


Figure 8. Hardness Vickers (HV2) and Young's modulus of the specimens.

As regards the tribological behaviour, the wear resistance and the coefficient of friction (COF) were measured and evaluated (Figures 9 and 10). The wear loss (mg) after sliding for 66.3 min (500 m, 400 rpm) is shown in Figure 9. This loss results differed significantly in their value due to the combination of B₄C and intermetallic content. The enhancement in fretting wear with only the addition of B₄C was relevant. It is important to note that the minor weight loss resulted in the TMC reinforced only with B₄C. The intermetallic incorporation in the starting powder involved that the weight loss increased by 50% and 53% in composites made from B₄C with Ti-Al(2) and Ti-Al(1), respectively. These phenomena were related to the amount of in situ formed TiB and TiC; if there were an obstacle to origin these secondary phases, the tribological properties could decline. Therefore, when the Al diffused into the matrix blocking these secondary reactions, there was less formation of TiB and TiC, which was reflected in the final tribological behaviour of the composites. These results were in agreement with the ones obtained by microscopy and XRD analysis.

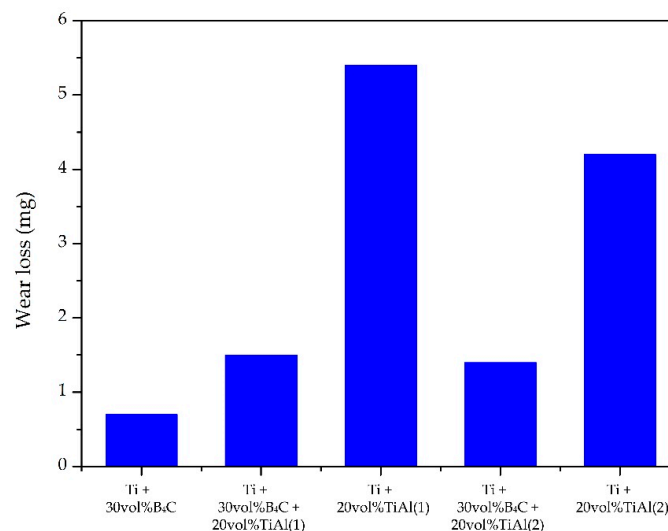


Figure 9. Wear loss vs. specimens.

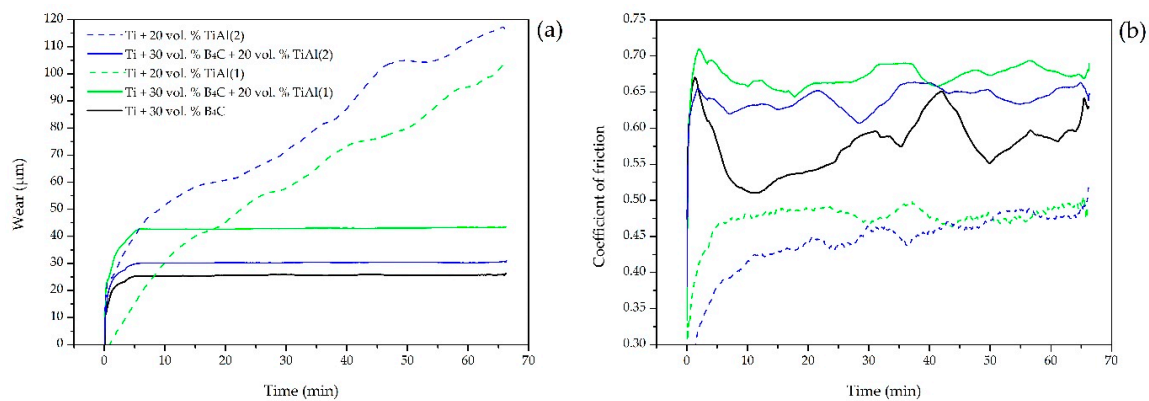


Figure 10. Tribology results: (a) wear vs. time and (b) coefficient of friction vs. time.

Figure 10 shows the wear and COF vs. time for all the specimens at the same wear conditions. In accordance with the commented above, the B₄C particles contributed to a lower penetration than in other specimens, as it can be appreciated in Figure 10a. In these specimens, the B₄C particles could participate in avoiding their pluck from the titanium matrix, maintaining the initial penetration corresponding to the applied load and speed. As expected, the absence of B₄C promoted the depth of the wear track, being the composite made from Ti-Al(2) the most affected. The COF vs. time is shown in Figure 10b. The coefficient values in the steady-state region were similar in specimens reinforced with B₄C. During the wear test, the particles and the hard precipitates in the titanium matrix could collide with the ball; therefore, COF was higher than in specimens without B₄C particles. Based upon the foregoing, when the intermetallic remained in the matrix, as in Ti-Al(1), there were also collisions between the ball and these precipitates, reflected in the COF values measured as seen in Figure 10b.

Optical micrographs in Figure 11 show representative worn track areas of the samples after the tribological characterisation. The composites with B₄C reinforcements seemed to be able to prevent the formation of severe worn surfaces, showing stronger behaviours. Moreover, in samples without ceramic reinforcements, Figure 11c,e, the material removal could be clearly appreciated with debris in the worn. The worn track surfaces were also significantly wider than in specimens with B₄C particles, being more noticeable when the intermetallic was added as an elementary blend.

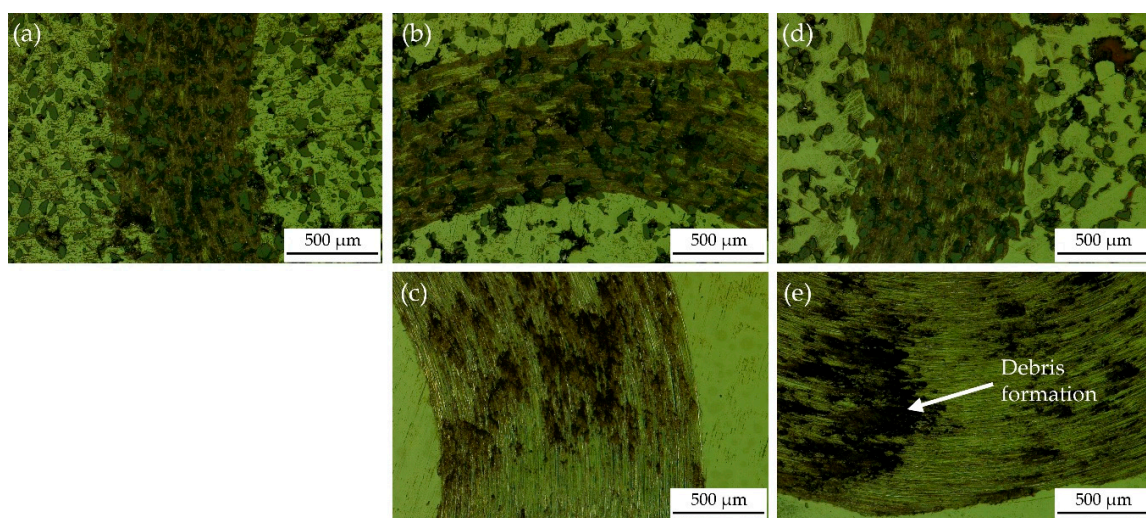


Figure 11. Worn surface: (a) Ti + 30 vol. % B₄C, (b) Ti + 30 vol. % B₄C + 20 vol. % Ti-Al(1), (c) Ti + 20 vol. % Ti-Al(1), (d) Ti + 30 vol. % B₄C + 20 vol. % Ti-Al(2) and (e) Ti + 20 vol. % Ti-Al(2).

4. Conclusions

The following conclusions were drawn from this research:

- (1) The presence of intermetallic affected considerably the formation of the secondary phases TiC and TiB. If the aluminium was added as an elementary powder in the blend, it caused less formation of these secondary phases, in comparison to the effect of the prealloyed Ti-Al powder. The presence of Al in the matrix could block the C and B diffusion, leading to a weak reaction between these elements and the titanium.
- (2) The reaction layers between B₄C and the matrix presented similar characteristics, regardless of the intermetallic powder in the blend. This reaction layer was narrower when only B₄C was used. When adding intermetallics, more TiB and TiC were accumulated around the ceramic particles due to the commented screen effect of Al in the matrix. The opposite occurred with the precipitates size of the secondary phases TiB and TiC being bigger when no intermetallic was added.
- (3) In relation to the reaction layer of the prealloyed Ti_xAl_y with titanium, a decomposition occurred allowing the Al to be introduced into the matrix.
- (4) Regarding the mechanical and tribological properties, composites with ceramic reinforcement showed excellent behaviour with high hardness values and good wear resistance. Without B₄C, the presence of prealloyed intermetallic in the matrix helped to a better performance than with the elementary Ti-Al blend.

Author Contributions: Authors have collaborated to obtain high-quality research work. Conceptualisation, E.N. and I.M.-M.; methodology, I.M.-M., E.M.P.S. and C.A.; formal analysis, I.M.-M.; investigation, C.A.; resources, M.K. and E.N.; data curation, E.M.P.S.; writing—original draft preparation, I.M.-M., E.M.P.S. and C.A.; writing—review and editing, C.A. and A.M.B.; visualisation, E.M.P.S. and funding acquisition, I.M.-M., E.M.P.S. and C.A. All authors have read and agreed to the published version of the manuscript.

Funding: The authors want to thank the Universidad de Sevilla for the use of experimental facilities at CITIUS, Microscopy and X-Ray Laboratory Services (VI PPIT-2018-I.5 Eva María Pérez Soriano, VI PPIT-2019-I.5 Cristina Arévalo Mora and VI PPIT-2019-I.5 Isabel Montealegre Meléndez).

Conflicts of Interest: The authors declare no conflicts of interest.

References

1. Lütjering, G.; Williams, J.C. *Titanium*, 2nd ed.; Springer: Berlin, Germany, 2007.
2. Leyends, C.; Peters, M. *Titanium and Titanium Alloys: Fundamentals and Applications*, 1st ed.; Wiley-VCH Verlag GmbH & Co. KGaA: Weinheim, Germany, 2003.
3. Elias, C.N.; Lima, J.H.C.; Valiev, R.; Meyers, M.A. Biomedical applications of titanium and its alloys. *JOM* **2008**, *60*, 46–49. [[CrossRef](#)]
4. Leary, M. Design of titanium implants for additive manufacturing. *Titan. Med. Dent. Appl.* **2018**, 203–224. [[CrossRef](#)]
5. Tjong, S.C.; Mai, Y.-W. Processing-structure-property aspects of particulate- and whisker-reinforced titanium matrix composites. *Compos. Sci. Technol.* **2008**, *68*, 583–601. [[CrossRef](#)]
6. Ravi Chandran, K.S.; Panda, K.B.; Sahay, S.S. TiB_w-reinforced Ti composites: Processing, properties, application prospects, and research needs. *JOM* **2004**, *56*, 42–48. [[CrossRef](#)]
7. Zadra, M.; Girardini, L. High-performance, low-cost titanium metal matrix composites. *Mater. Sci. Eng. A* **2014**, *608*, 155–163. [[CrossRef](#)]
8. Neubauer, E.; Vály, L.; Kitzmantel, M.; Grech, D.; Rovira, A.; Montealegre-Meléndez, I.; Arévalo, C. Titanium Matrix Composites with High Specific Stiffness. *Key Eng. Mater.* **2016**, *704*, 38–43. [[CrossRef](#)]
9. Cao, Z.; Wang, X.; Li, J.; Wu, Y.; Zhang, H.; Guo, J.; Wang, S. Reinforcement with graphene nanoflakes in titanium matrix composites. *J. Alloys Compd.* **2017**, *696*, 498–502. [[CrossRef](#)]
10. Sabahi Namini, A.; Azadbeh, M.; Shahedi Asl, M. Effect of TiB₂ content on the characteristics of spark plasma sintered Ti–TiB_w composites. *Adv. Powder Technol.* **2017**, *28*, 1564–1572. [[CrossRef](#)]

11. Montealegre-Meléndez, I.; Neubauer, E.; Angerer, P.; Danninger, H.; Torralba, J.M. Influence of nano-reinforcements on the mechanical properties and microstructure of titanium matrix composites. *Compos. Sci. Technol.* **2011**, *71*, 1154–1162. [[CrossRef](#)]
12. Zhang, X.; He, M.; Yang, W.; Wu, K.; Zhan, Y.; Song, F. Structure and mechanical properties of in-situ titanium matrix composites with homogeneous Ti₅Si₃ equiaxial particle-reinforcements. *Mater. Sci. Eng. A* **2017**, *698*, 73–79. [[CrossRef](#)]
13. Ni, D.R.; Geng, L.; Zhang, J.; Zheng, Z.Z. Effect of B₄C particle size on microstructure of in situ titanium matrix composites prepared by reactive processing of Ti–B₄C system. *Scr. Mater.* **2006**, *55*, 429–432. [[CrossRef](#)]
14. Zhang, Y.; Sun, J.; Vilar, R. Characterization of (TiB+TiC)/TC4 in situ titanium matrix composites prepared by laser direct deposition. *J. Mater. Process. Technol.* **2011**, *211*, 597–601. [[CrossRef](#)]
15. Arévalo, C.; Kitzmantel, M.; Neubauer, E.; Montealegre-Meléndez, I. Development of Ti-MMCs by the use of different reinforcements via conventional Hot-Pressing. *Key Eng. Mater.* **2016**, *704*, 400–405. [[CrossRef](#)]
16. Wang, X.; Wang, L.; Luo, L.; Yan, H.; Li, X.; Chen, R.; Su, Y.; Guo, J.; Fu, H. High temperature deformation behavior of melt hydrogenated (TiB+TiC)/Ti-6Al-4V composites. *Mater. Des.* **2017**, *121*, 335–344. [[CrossRef](#)]
17. Jia, L.; Li, S.; Imai, H.; Chen, B.; Kondoh, K. Size effect of B₄C powders on metallurgical reaction and resulting tensile properties of Ti matrix composites by in-situ reaction from Ti–B₄C system under a relatively low temperature. *Mater. Sci. Eng. A* **2014**, *614*, 129–135. [[CrossRef](#)]
18. Radhakrishna Bhat, B.V.; Subramanyam, J.; Bhanu Prasad, V.V. Preparation of Ti-TiB-TiC & Ti-TiB composites by in-situ reaction hot pressing. *Mater. Sci. Eng. A* **2002**, *325*, 126–130. [[CrossRef](#)]
19. AlMangour, B.; Grzesiak, D.; Yang, J.-M. In-situ formation of novel TiC-particle-reinforced 316L stainless steel bulk-form composites by selective laser melting. *J. Alloys Compd.* **2017**, *706*, 409–418. [[CrossRef](#)]
20. Jia, L.; Wang, X.; Chen, B.; Imai, H.; Li, S.; Lu, Z.; Kondoh, K. Microstructural evolution and competitive reaction behavior of Ti-B₄C system under solid-state sintering. *J. Alloys Compd.* **2016**, *687*, 1004–1011. [[CrossRef](#)]
21. Li, S.; Kondoh, K.; Imai, H.; Chen, B.; Jia, L.; Umeda, J. Microstructure and mechanical properties of P/M titanium matrix composites reinforced by in-situ synthesized TiC–TiB. *Mater. Sci. Eng. A* **2015**, *628*, 75–83. [[CrossRef](#)]
22. Arévalo, C.; Montealegre-Meléndez, I.; Ariza, E.; Kitzmantel, M.; Rubio-Escudero, C.; Neubauer, E. Influence of Sintering Temperature on the Microstructure and Mechanical Properties of In Situ Reinforced Titanium Composites by Inductive Hot Pressing. *Materials* **2016**, *9*, 919. [[CrossRef](#)]
23. Ma, F.; Shi, Z.; Liu, P.; Li, W.; Liu, X.; Chen, X.; He, D.; Zhang, K.; Pan, D.; Zhang, D. Strengthening effect of in situ TiC particles in Ti matrix composite at temperature range for hot working. *Mater. Charact.* **2016**, *120*, 304–310. [[CrossRef](#)]
24. Ma, F.; Wang, T.; Liu, P.; Li, W.; Liu, X.; Chen, X.; Pan, D.; Lu, W. Mechanical properties and strengthening effects of in situ (TiB+TiC)/Ti-1100 composite at elevated temperatures. *Mater. Sci. Eng. A* **2016**, *654*, 352–358. [[CrossRef](#)]
25. Zhao, Q.; Liang, Y.; Zhang, Z.; Li, X.; Ren, L. Effect of Al content on impact resistance behavior of Al-Ti-B₄C composite fabricated under air atmosphere. *Micron* **2016**, *91*, 11–21. [[CrossRef](#)] [[PubMed](#)]
26. Zhang, J.; Lee, J.-M.; Cho, Y.-H.; Kim, S.-H.; Yu, H. Effect of the Ti/B₄C mole ratio on the reaction products and reaction mechanism in an Al–Ti–B₄C powder mixture. *Mater. Chem. Phys.* **2014**, *147*, 925–933. [[CrossRef](#)]
27. Schmidt, J.; Boehling, M.; Burkhardt, U. Preparation of titanium diboride TiB₂ by spark plasma sintering at slow heating rate. *Sci. Technol. Adv. Mater.* **2007**, *8*, 376–382. [[CrossRef](#)]
28. Kondoh, K. 16—Titanium metal matrix composites by powder metallurgy (PM) routes. In *Titanium Powder Metallurgy*; Qian, M., Froes, F.H., Eds.; Butterworth-Heinemann: Oxford, UK, 2015; pp. 277–297.
29. Montealegre-Meléndez, I.; Neubauer, E.; Arévalo, C.; Rovira, A.; Kitzmantel, M. Study of Titanium Metal Matrix Composites Reinforced by Boron Carbides and Amorphous Boron Particles Produced via Direct Hot Pressing. *Key Eng. Mater.* **2016**, *704*, 85–93. [[CrossRef](#)]
30. Montealegre-Meléndez, I.; Arévalo, C.; Perez-Soriano, E.M.; Kitzmantel, M.; Neubauer, E. Microstructural and XRD Analysis and Study of the Properties of the System Ti-TiAl-B₄C Processed under Different Operational Conditions. *Metals* **2018**, *8*, 367. [[CrossRef](#)]
31. ASM-International. *Nondestructive Evaluation and Quality Control*, 9th ed.; ASM-International: Materials Park, OH, USA, 1989.

32. ASTM C373-14. *Standard Test Method for Water Absorption, Bulk Density, Apparent Porosity, and Apparent Specific Gravity of Fired Whiteware Products, Ceramic Tiles, and Glass Tiles*; ASTM International: West Conshohocken, PA, USA, 2014.
33. Okulov, A.V.; Volegov, A.S.; Weissmüller, J.; Markmann, J.; Okulov, I.V. Dealloying-Based Metal-Polymer Composites for Biomedical Applications. *Scr. Mater.* **2018**, *146*, 290–294. [[CrossRef](#)]
34. Okulov, I.V.; Okulov, A.V.; Volegov, A.S.; Markmann, J. Tuning Microstructure and Mechanical Properties of Open Porous TiNb and TiFe Alloys by Optimization of Dealloying Parameters. *Scr. Mater.* **2018**, *154*, 68–72. [[CrossRef](#)]
35. Okulov, I.V.; Sarmanova, M.F.; Volegov, A.S.; Okulov, A.; Kühn, U.; Skrotzki, W.; Eckert, J. Effect of Boron on Microstructure and Mechanical Properties of Multicomponent Titanium Alloys. *Mater. Lett.* **2015**, *158*, 111–114. [[CrossRef](#)]
36. Okulov, I.V.; Bönisch, M.; Okulov, A.V.; Volegov, A.S.; Attar, H.; Ehteram-Haghighi, S.; Calin, M.; Wang, Z.; Hohenwarter, A.; Kaban, I.; et al. Phase Formation, Microstructure and Deformation Behavior of Heavily Alloyed TiNb- and TiV-Based Titanium Alloys. *Mater. Sci. Eng. A* **2018**, *733*, 80–86. [[CrossRef](#)]



© 2020 by the authors. Licensee MDPI, Basel, Switzerland. This article is an open access article distributed under the terms and conditions of the Creative Commons Attribution (CC BY) license (<http://creativecommons.org/licenses/by/4.0/>).